Received: 21 January 2025 Revised: 3 March 2025 Accepted: 3 March 2025
DOI: https://doi.org/10.29244/primatology.3.01.37-45 E-ISSN: 2964-5441

RESEARCH ARTICLE

INAJP INDONESIAN JOURNAL OF PRIMATOLOGY

Histopathological Analysis of *Pseudomonas putida* Infection in *Macaca fascicularis*

Shanice Andrea Knight[1*], Huda S. Darusman[1,2], Bambang Pontjo Priosoeryanto[1], Silvia A. Prabandari[2]

[1]School of Veterinary Medicine and Biomedical Sciences, IPB University. Jl. Agatis, Kampus IPB Dramaga, Bogor, Indonesia
[2]Primate Research Center, Institute of Research and Community Services, IPB University. Jl. Lodaya II No. 5, Bogor, Indonesia

Abstract

Pseudomonas putida is a gram-negative, rod-shaped, flagellated bacterium found in soil and water. The bacteria were obtained through bacterial culture from organ swabs of cynomolgus monkeys (*Macaca fascicularis*). This study aimed to evaluate and analyse histological slides of *Macaca fascicularis* organs, including the liver, kidneys, lungs, and spleen, which were suspected to be infected with *Pseudomonas putida*. The most common lesion was necrosis, which was observed in the lungs, liver, and spleen. Another lesion found in the liver, lungs, and kidneys is congestion around the cells, whereas haemorrhages can be found in the red pulp and capsules of the spleen and in the tubules of the kidneys. Abundant inflammatory cells were found in all organ samples, such as the liver, lungs, spleen, and kidneys, as all organs were infected with bacteria. The last lesion in the lung sample was a benign pulmonary nodular lesion. Based on histopathological analysis, we concluded that the lungs were the organs most affected by *P. putida* infection, whereas the kidneys were the least affected.

Keywords: histopathological, internal organs, *Macaca fascicularis*, *Pseudomonas putida*

1. Introduction

Bacteria of the genus *Pseudomonas* are ubiquitous in soil, water, plant surfaces and animal tissues. This genus belongs to the gamma subclass of Proteobacteria and is chemo-organotrophic aerobic, which has gram-negative rods with polar flagella and respiratory metabolism rather than fermentative metabolism (Palleroni 1984).

Pseudomonas putida is a rod-shaped, flagellated, gram-negative bacterium found in most soil and water habitats. It grows optimally at 25-30°C and can be easily isolated. *P. putida* has several strains, including the KT2440, which colonises the plant roots in which there is a mutual relationship between the plant and bacteria. Strains of *P. putida* are frequent rhizosphere and freshwater inhabitants that exhibit a remarkable ability to metabolise a wide range of biogenic and xenobiotic compounds (Fernández *et al*. 2012; Udaondo *et al*. 2013).

Several strains of this species have been isolated from patients who acquired infections in hospital environments. Infections caused by *P. putida* are rare and are primarily reported in immuno-compromised individuals, such as those with neutropenia, newborns, and cancer patients (Lombardi *et al*. 2002; Kim *et al*. 2012; Erol *et al*. 2014). Most isolates exhibit resistance to certain antibiotics through the presence of plasmids bearing genes that encode antibiotic resistance factors (Molina *et al*. 2014), which can be transferred to other microorganisms in hospital environments (Martino *et al*. 1996; Yoshino *et al*. 2011).

Although *P. putida* may cause healthcare-related infections, clinical data on *P. putida* infections are scarce. This is likely due to the rarity, relatively lower virulence, and higher antimicrobial susceptibility of *P. putida* compared to *P. aeruginosa* (Blazevic *et al*. 1973; Carpenter *et al*. 2008; Yoshino *et al*. 2011).

The reason for using a non-human primate model, such as *Macaca fascicularis*, in this experiment to identify the pathological lesion of *Pseudomonas putida* is that non-human primates share physiological similarities with humans; therefore, studying the infection in this monkey may help to understand the pathogen's infection or to model the infection in humans.

2. Materials and Methods

2.1 Time and Place

The experiment was conducted in the Pathology Laboratory, Primate Research Centre (PSSP), IPB University at Lodaya-Bogor.

2.2 Equipment and Materials

The equipment used in this research included a minor surgical set, cassettes, beakers, object glasses, cover slips, embedding tissue console, microtome, water bath, incubator, staining jar, timer, and light microscope with an attached camera (Nikon Eclipse 80i DS Fi1, Japan). The materials used in this research are *Macaca fascicularis* organs such as the liver, kidneys, spleen, and lungs, 10% neutral buffered formalin (NBF) as a fixative solution, 0.9% NaCl physiological solution, alcohol, xylol, liquid paraffin, haematoxylin and eosin stains, adhesive ethylene media, and distilled water.

*Corresponding author
Email Address : shaniceandrea.0710@gmail.com

2.3 Procedures

2.3.1 Direct Sampling

The bacteria were identified through bacterial culture by a PSSP IPB University pathologist. Samples, such as the lungs, liver, spleen, and kidneys, were collected from cynomolgus monkeys. Each organ was cut into approximately 2 cm in length and 0.5 cm in thickness to fit into cassettes. The cut organs were then placed in different cassettes and labelled. The organs were then further fixed, dehydrated, cleared, and stained for several more processes up to micro-photography.

2.3.2 Histology Procedure

The cassettes were fixed using a 10% neutral buffered formalin (NBF) solution. The samples were then rinsed with running water and soaked in water for a few minutes. Dehydration was performed by placing the prepared cassettes in a carousel with increasing percentages of alcohol, from 70% to 100%, to remove the water content in the organs. Each step was performed in approximately an hour. The next step is clearing. This process was performed by soaking the samples in xylene three times: xylene I, II, and III. Each step was performed for approximately an hour, at room temperature to clear the tissue and fill the water content of tissues/cells that had been removed previously. The samples soaked in xylene I, xylene II, and xylene III were then incubated at 60-63ºC for another 60 min for further paraffin melting.

The embedding process was divided into a few steps: reusable stainless-steel base moulds were prepared according to the sample dimensions. Reusable stainless-steel base moulds were filled with hot paraffin and placed on an embedding tissue console on a hot plate. The samples were placed in a reusable stainless-steel base mould filled with paraffin. The part with lesions was placed facing the bottom of the stainless-steel mould, and the samples were pressed. The reusable stainless-steel base mould was then placed on a cooling plate to freeze the paraffin, forming paraffin blocks. The tissue block was cut using a Rotary Microtome 820 Spencer. The goal is to obtain thin pieces of tissue with a micro thickness (5µm) to observe them properly using a microscope.

2.3.3 Staining

The staining carried out on the tissue preparations was the general staining of Haematoxylin Eosin (HE). Haematoxylin dye solution stains the cell nucleus, whereas eosin stains the cytoplasm.

2.4 Photomicrography and Result Analysis

Morphological observations were performed using a light microscope with several objective lens magnifications (4x, 10x, and 40x). Photomicrographs were obtained using photomicrographic equipment equipped with a scale bar on each photo with different scale lengths for each calibrated objective lens magnification (Nikon Eclipse 80i DS Fi1, Japan). The data collected were qualitative, as the abnormalities and lesions were observed and described in words.

3. Results

3.1 Liver

According to the microscopy observations, a few lesions were found in the liver. The most apparent lesion was a necrotic area (Figure 1), where hepatocytes were not visible. Another lesion observed in the liver samples was congestion around the sinusoidal space (Figure 2). Haemorrhages were also found in the sample, as no clear signs of erythrocytes were observed. Other lesions, such as inflammation in the portal vein, can also be found in the sample, as inflammatory cells are abundant.

3.2 Lungs

An apparent histopathological change was found in the lung samples, as one of the common symptoms of *Pseudomonas sp.* infection is pneumonia, which mainly affects the lungs of the infected macaque. The results showed that the alveoli were swollen as they were filled with exudate, thus rupturing the lining of the alveolar septum (Figure 3). This condition is known as alveolar pneumonia. Congestion was also observed in the alveoli and bronchi of the lungs (Figure 4). Another lesion found in this sample was pulmonary nodules, which were infiltrated by inflammatory cells.

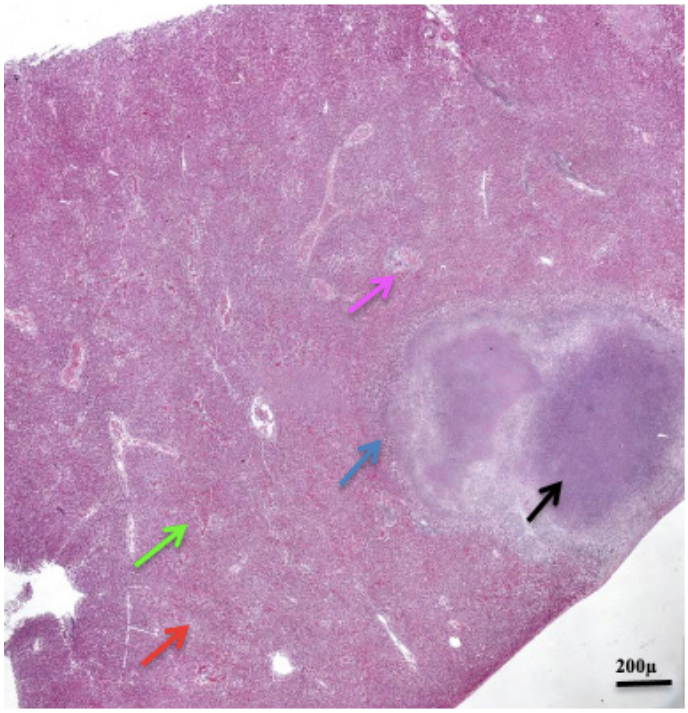

Figure 1. Histopathological image of the liver at magnification objective lens 4x. Black arrow: necrotic area; blue arrow: border between necrotic and clear border; purple arrow: triad (bile ductule, hepatic artery, portal vein); green arrow: sinusoid filled with congestion; red arrow: large hepatocyte space.

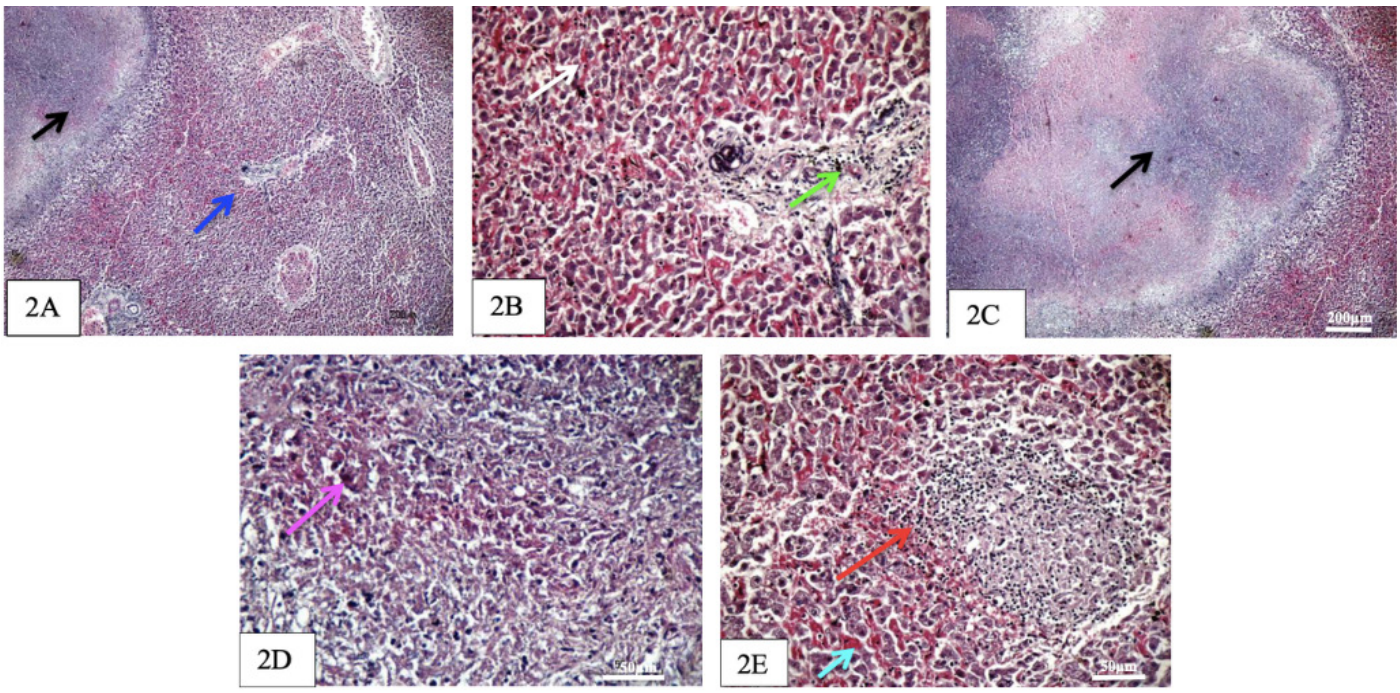

Figure 2. Histopathological image of liver. 2A, black arrow: necrotic area; blue arrow: inflamed portal vein, at magnification of objective lens 4x (200µm scale). 2B, white arrow: sinusoid filled with congestion; green arrow: abundant inflammatory cells, at a magnification of 20x (50µm scale). 2C, black arrow: necrotic area, at a magnification of 20x (200µm scale). 2D, purple arrow: large hepatocyte space, at a magnification of 20x (50µm scale). 2E, red arrow: central vein inflamed; light blue arrow: congestion in sinusoid, at magnification of objective lens 20x (50µm scale).

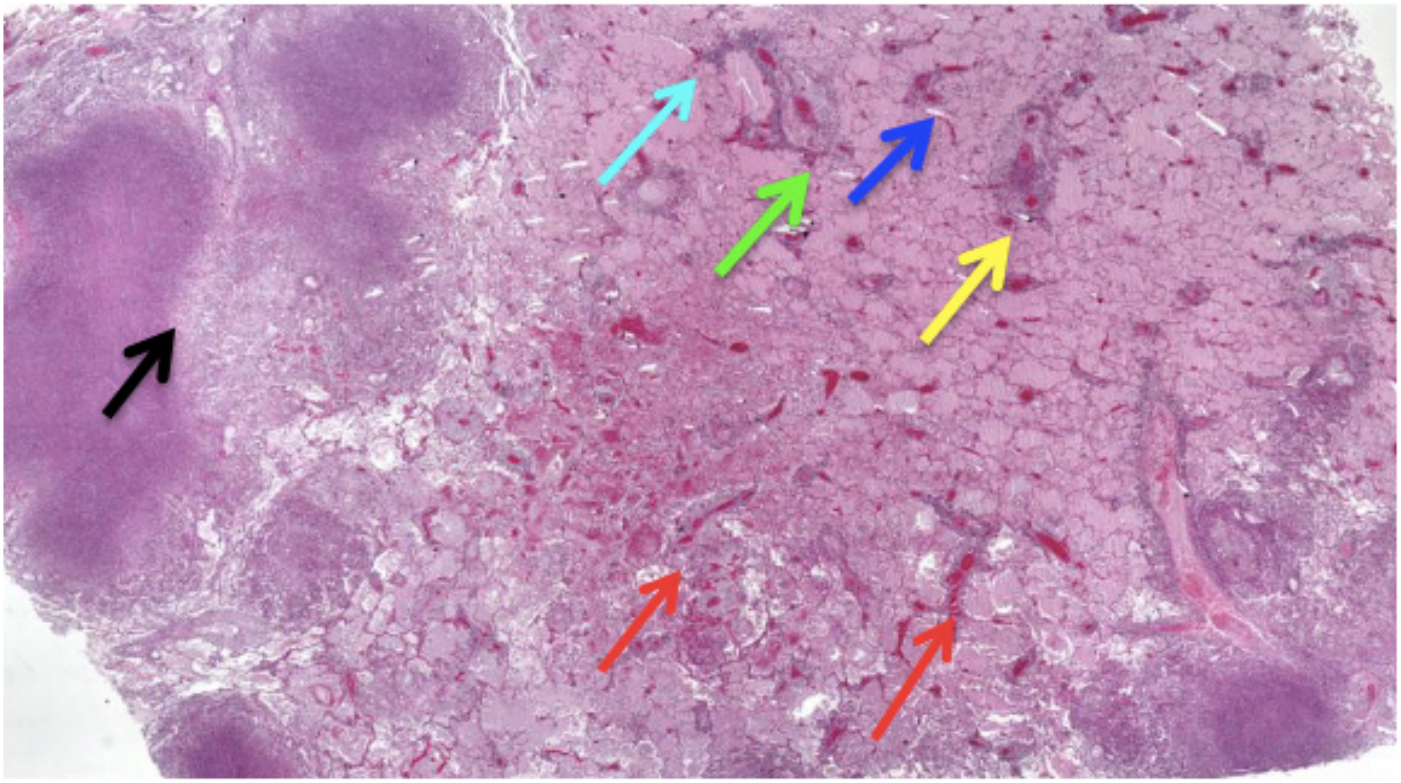

Figure 3. Histopathological image of lungs at a magnification of 4x. Black arrow: cell necrosis; lightblue arrow: exudate in alveolar; blue arrow: lining of alveolar septum rupture; green arrow: pneumonia interstitialis; yellow arrow: inflamed nodule; purple arrow: inflamed bronchus; red arrow: congestion in blood vessel.

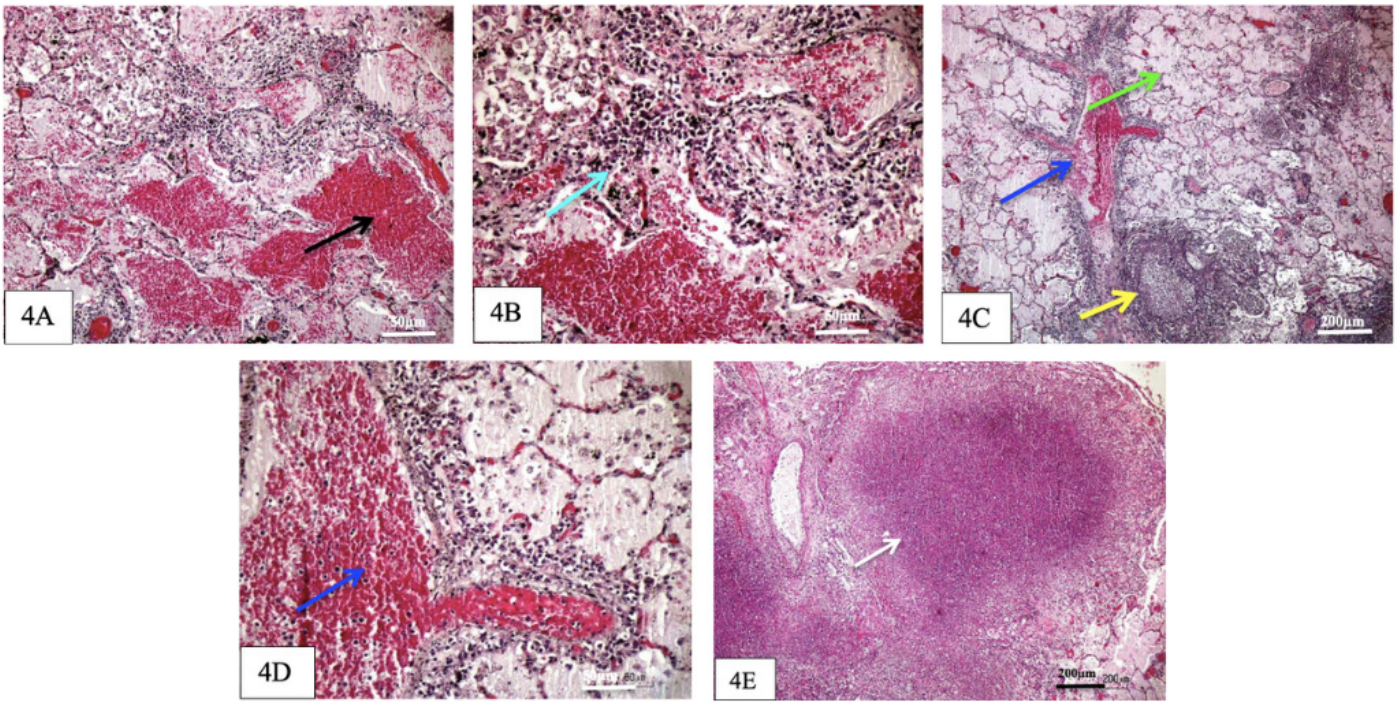

Figure 4. Histopathological image of the lungs. 4A, black arrow: congestion filled with RBCs, at a magnification of 4x (50µm scale). 4B, light blue arrow: abundant inflammatory cells at a magnification of 20x (50µm scale). 4C, blue arrow: congestion in the bronchus; green arrow: lining septum of alveolar rupture; yellow arrow: granulated nodules, at a magnification of 4x (200µm scale). 4D, blue arrow: congestion in the bronchus, at a magnification of 20x (50µm scale). 4E, white arrow: necrotic area, at a magnification of objective lens 4x (200µm scale).

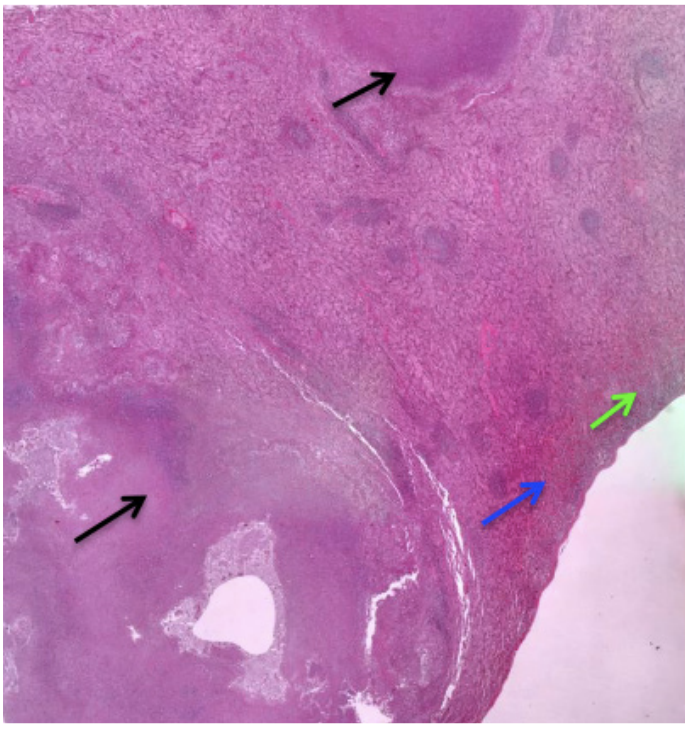

Figure 5. Histopathological image of the spleen at a magnification of 4x. Black arrow: necrotic area; blue arrow: congestion in red pulp and capsule; green arrow: abundant inflammatory cells.

3.3 Spleen

One of the most common lesions found in the samples was splenic necrosis (Figure 5 and 6). Haemorrhage can also be found around the red pulp of the spleen. There are also abundant inflammatory cells around the red pulp of the spleen. The spleen sample was darker in colour and appeared more complex in texture. Necrotic areas were also observed in the spleen.

3.4 Kidneys

A few lesions were observed in the kidneys under a light microscope. As observed in the left renal photomicrograph, haemorrhages were found between the distal and proximal convoluted tubules in the cortex (Figures 7 and 8). Congestion was also observed in the subscapular vein and Bowman's capsule (Figure 8). Abundant inflammatory cells were also observed around the proximal and distal tubules. However, fewer lesions were observed in the right kidney photomicrograph. There were abundant inflammatory cells around the tubule space (Figure 9 and 10), which were clearly visible, although it was difficult to identify the types of inflammatory cells.

The compilation of all microscopic lesions in each organ is summarised in Table 1.

4. Discussion

According to Al-Mossawai (2019), the histopathological changes in the liver post-*Pseudomonas* sp. infection were characterised by vacuolation, inflammatory cells, and haemorrhage, while necrosis and swelling of hepatocytes and infiltration with inflammatory cells usually occur post-infection. As observed in the photomicrograph,

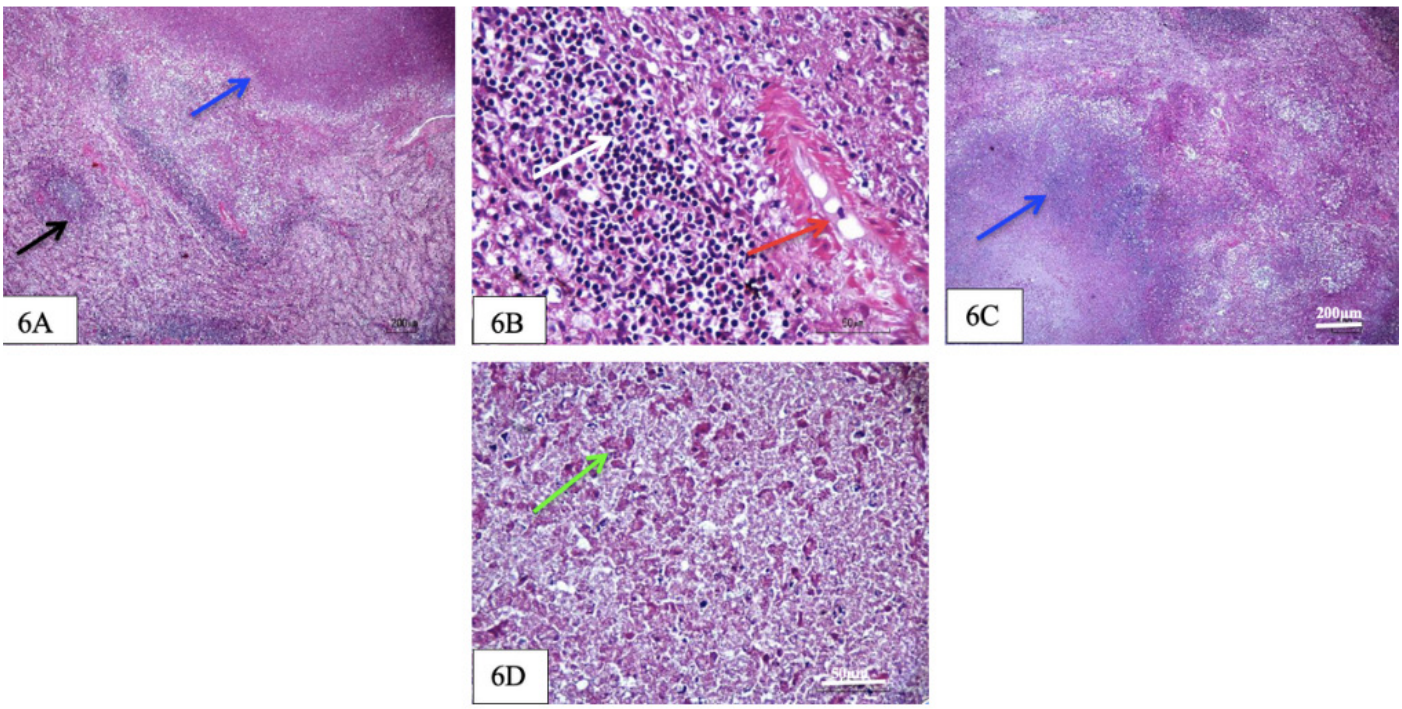

Figure 6. Histopathological image of the spleen. 6A, black arrow: white pulp; blue arrow: necrotic area, at a magnification of objective lens 4x (200µm scale). 6B, red arrow: trabecula; white arrow: abundant inflammatory cells, at a magnification of 40x (50µm scale). 6C, blue arrow: necrotic area, at a magnification of objective lens 4x (200µm scale). 6D, green arrow: congestion in the red pulp, at a magnification of 40x (50µm scale).

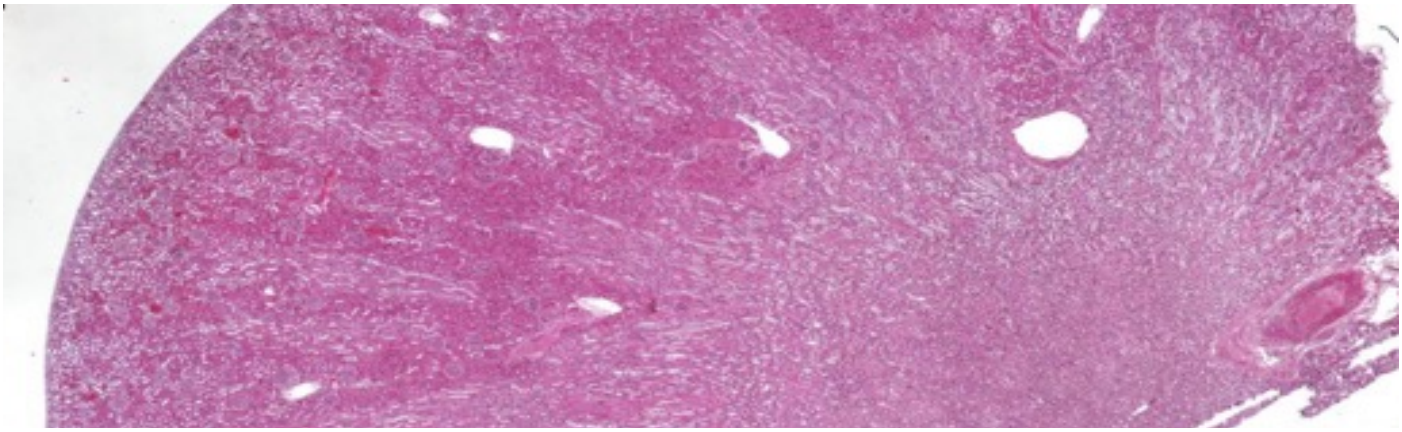

Figure 7. Histopathological image of the left kidney at magnification of objective lens 4x, congestion between distal and proximal tubules.

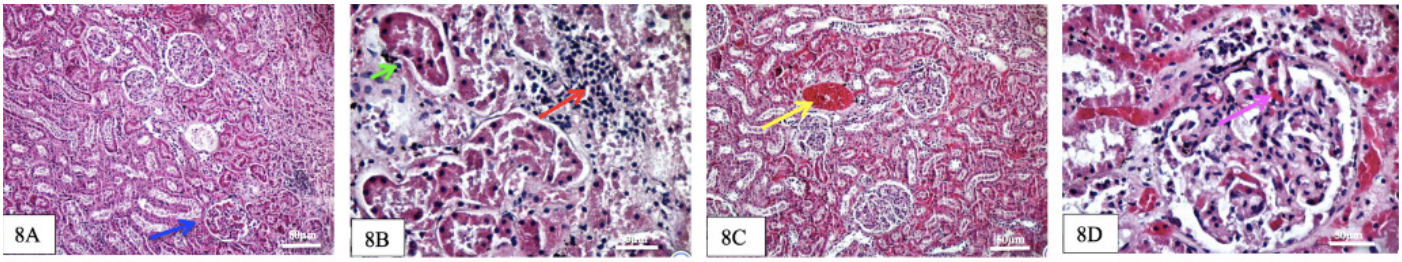

Figure 8. Histopathological image of the left kidney at 50µm scale. 8A, blue arrow: haemorrhage in Bowman's capsule (podocytes), at magnification of objective lens 10x. 8B, green arrow: haemorrhage in distal convoluted tubules; red arrow: abundant inflammatory cells, at magnification of objective lens 40x. 8C, yellow arrow: congestion in the subscapular vein, at a magnification of 10x. 8D, pink arrow: congestion in Bowman's capsule, at a magnification of 40x.

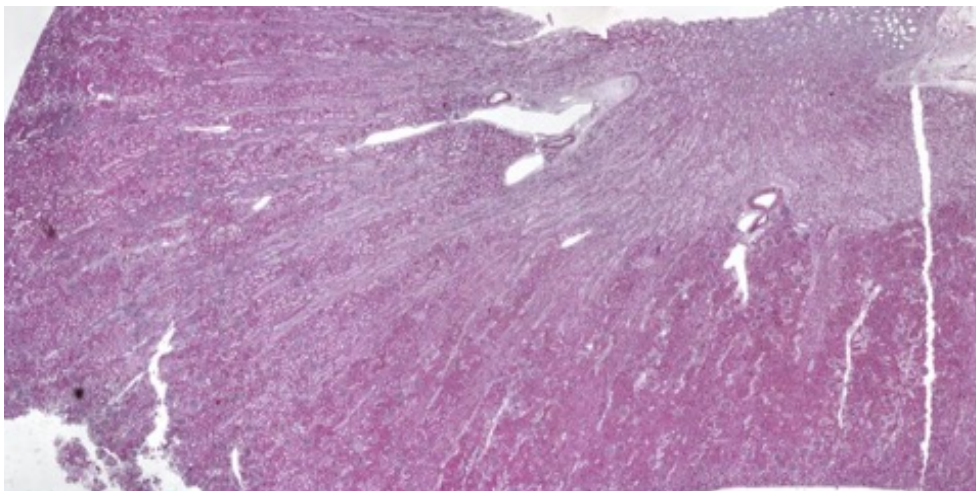

Figure 9. Histopathological image of the right kidney at a magnification of 4x.

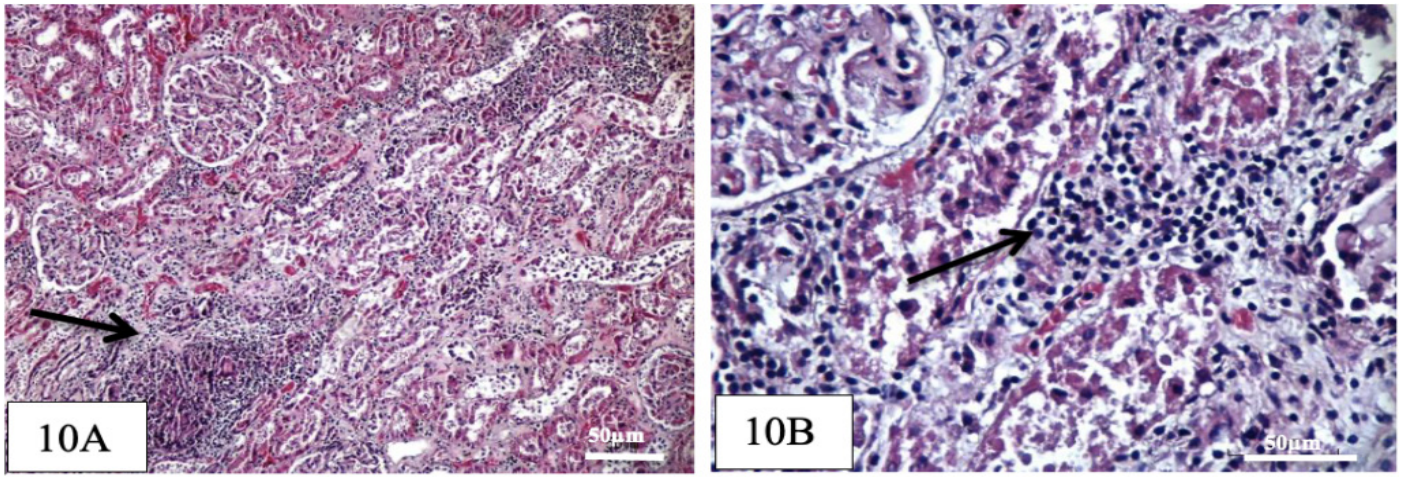

Figure 10. Histopathological image of the right kidney at 50µm scale. 10A, black arrow: abundant inflammatory cells around the tubule space, at a magnification of 4x. 10B, black arrow: abundant inflammatory cells around the tubule space, at a magnification of 40x.

Table 1. Comparison of lesions in each organ of *Macaca fascicularis* which were suspected to be infected with *Pseudomonas putida*

Lesion	Organs			
	Liver	Lungs	Spleen	Kidneys
Necrosis	+	+	+	-
Congestion	+	+	-	+
Haemorrhages	+	-	+	+
Inflammation	+	+	+	+
Exudate in alveolar	-	+	-	-
The alveolar septum's lining rupture	-	+	-	-

The mark (+) indicates the presence of a lesion in each organ.

the results can be attributed to post-*Pseudomonas* sp. infection, as there is necrosis and infiltration of inflammatory cells. However, haemorrhages and congestion were also observed in the samples.

The necrotic area observed in the histopathological examination of the sample was relatively obvious compared to the pathological lesion. According to Krasnogorskiĭ *et al*. (1983), the livers of patients infected with *Pseudomonas* sp. presented foci of necrosis of different sizes with tremendous numbers of bacteria. Furthermore, haemorrhages in histopathological view can also be seen pathologically as the liver sample appears darker. However, no hepatomegaly was observed pathologically.

Cell necrosis is an irreversible injury to cells due to encounters with noxious stimuli, which invariably leads to cell death. This can be caused by external factors, including infectious agents (bacteria, viruses, fungi, and parasites), hypoxia, and extreme environmental conditions, such as heat, radiation, or exposure to ultraviolet irradiation. Necrosis is a common finding in acute or chronic liver disease,

with the persistence of underlying causes, which can be followed by progressive fibrosis.

During a liver biopsy, the extent and pattern of necrosis are observed, as the degree of inflammation is often considered. The pattern and extent of necrosis were evaluated in the context of morphological changes to determine or estimate the underlying causes (Ludwig *et al*. 1998). From the results obtained, it can be deduced that the pattern of necrosis in this sample is zonal necrosis, as a clear border can be seen between the necrotic and normal areas (Figure 2). Zonal necrosis often refers to necrosis involving a particular zone of the acinus, such as centrilobular necrosis resulting from ischaemic or drug-related injury (Lefkowitch 2007).

Congestion around the sinusoidal space is known as hepatic sinusoidal dilation, which is often caused by hepatic venous outflow impairment, resulting in vascular stasis and congestion of the hepatic parenchyma (Brancatelli *et al*. 2018). This impairment can occur at the level of the small hepatic veins (veno-occlusive disease), large hepatic veins (Budd-Chiari syndrome), or the heart (right-sided heart failure, tricuspid valve disease, and constrictive pericarditis), and is often accompanied by hepatocyte atrophy. However, sinusoidal dilatation and congestion can also occur due to systemic inflammatory diseases, granulomatous disorders, as well as neoplasms (Bruguera *et al*. 1978).

Histopathological descriptions of lung injury in acute *P. aeruginosa* infections vary depending on the patient and the mode of infection. Lesions in nosocomially acquired necrotising pneumonia are characterised by alveolar septal necrosis with necrosis of the arterial walls and secondary thrombosis (Mays *et al*. 1969). This can also be seen in the histopathological lesions in the lung samples affected by *P. putida*, which are alveolar pneumonia and rupture of the alveolar septum. The principal microscopic finding in cases of *P. aeruginosa* pneumonia acquired after bacteraemia originating from another site is intra-alveolar haemorrhage with patchy alveolar septal necrosis (Fetzer *et al*. 1967). However, congestion was observed in the lung samples instead of haemorrhage, as obvious erythrocytes were observed microscopically.

The pathology of community-acquired pneumonia caused by *P. aeruginosa* is characterised by multiple small abscesses and marked alveolar cell necrosis (Tillotson 1968). According to the pathological lesions, the lungs appeared darker and more elastic, whereas a necrotic area was observed in the lung sample with an abscess. Congestion may result in a darker appearance of the lungs. *Pseudomonas pneumonia* due to haematogenous spread is characterised by areas of necrosis that are usually surrounded by a red halo of congestion and haemorrhage, which go on to form cavities (Farver 2018).

Histopathologically, pneumonia can be divided into lobar pneumonia and bronchopneumonia. Lobar pneumonia is characterised by diffuse consolidation involving the entire lobe of the lung. This process can be divided into four stages: congestion, red hepatisation, grey hepatisation, and resolution (Löffler *et al*. 2014). In this case, pneumonia is known as pseudo-lobular pneumonia because up to 2/3 of the lobe of the lungs is affected. Congestion occurs when the alveoli accumulate infective organisms, and few erythrocytes and neutrophils are observed at this stage. Erythrocytes, neutrophils, and fibrin infiltration mark red hepatization into the alveolar fluid. Hepatisation refers to the grossly red and firm appearance of the lung, whereas in grey hepatisation, the erythrocytes break down and associate with fibrinopurulent exudate, causing a red-to-grey colour transformation to the lungs (Hussain *et al*. 2005).

Furthermore, congestion was observed in the bronchus. An increase in flow or blood volume, but a reduction in flow due to high cardiac filling pressure and/or high pulmonary vascular pressure, can occur due to congestion in the bronchial circulation. This can lead to thickened bronchial mucosal and submucosal tissues and reduced airway compliance, resulting in airway obstruction, restriction, and a lack of airway distensibility (Ceridon *et al*. 2009).

There are two main types of pulmonary nodules: malignant and benign ones. Benign pulmonary nodules usually result from infection or disease-induced inflammation in the body. The nodule may represent an active process or result from scar tissue formation related to previous inflammation. Benign developmental lesions can also appear as nodules. Inflammation associated with infections, often known as granuloma, is a small lump of cells that forms when lung tissue is inflamed. It usually forms when the immune system isolates foreign substances, such as bacteria, such as *P. putida* (Allen 2003).

According to Baraaj (2013), intraperitoneal injection of *P. aeruginosa* DNA in rats caused several histopathological changes in the splenic tissue, including marked germinal centre hyperplasia in the white pulp, which resulted in an increase in the number of follicles within the germinal centre. Furthermore, apoptotic debris engulfed by macrophages in the marginal zone was observed. Hemosiderin and degenerated cells were also observed. The histopathological results showed that the white pulp was normal. However, inflammatory cells infiltrated the red pulp of the spleen in the sample, which could be due to macrophage infiltration. Hemosiderin was not detected in the spleen samples.

It was suspected that the haemorrhage in the organ sample was congested; therefore, the spleen might appear darker. Theoretically, chronic melioidosis can occur in the spleen, followed by necrosis (Ashdown 1984). Furthermore, splenic abscesses can occur due to *Pseudomonas* infections. Almost all splenic abscesses develop due to bacteraemia (or fungaemia), although a small percentage spread to the spleen from contiguous sites. The necrotic area found in the spleen sample can also be due to a splenic abscess. The gross pathology of *P. aeruginosa* in the spleen of mice showed spleen enlargement with ascites (Shaheed 2018). However, no enlargement of the

spleen sample was collected for this study, and ascites were not found.

Necrosis is often associated with trauma, obstruction, or neoplasia. Splenic necrosis can be characterised by cell swelling, condensation and dissolution of the nucleus, and cell lysis with the accumulation of eosinophilic cytoplasmic and karyorrhectic nuclear debris (Figure 6). Moreover, inflammation, haemorrhage, fibrin, fibrosis, and/or mineralisation may accompany splenic necrosis (Suttie 2006). However, inflammatory cells could not be observed in this photomicrograph because the resolution and magnification were not optimal for further observations.

Haemorrhages can also be found around the red pulp of the spleen, which is caused by extravasated erythrocytes within the splenic capsule or parenchyma. Splenic haemorrhages can be distinguished from angiectasis, congestion, haemangioma, and hemangiosarcoma. Angiectasis is usually a focal lesion associated with an area of fibrosis, whereas congestion is usually found in the sinuses of the red pulp and may or may not have an identifiable cause.

Haemangiomas and hemangiosarcomas are neoplasms of the splenic vascular endothelium (Stefanski *et al*. 1990). It is predicted that the haemorrhages found in this sample could be congested. However, erythrocytes were not entirely visible in the photomicrographs. No amyloidosis was observed in the spleen samples.

According to Oh *et al*. (2019), there was degeneration of tubules surrounded by lymphocytes and macrophages in the kidneys of rainbow trout infected with a strain of *P. structure*, which was classified as *P. putida*. Signs of phagocytosed rod-shaped bacteria and cellular debris were also observed in the kidney samples. Hyaline droplet accumulation was also observed in the tubular epithelium of the kidneys of diseased fish. Furthermore, diverse immunocytes, including lymphocytes and macrophages, infiltrated the surrounding tubules. However, in this study, only the infiltration of inflammatory cells was observed around the tubule space of the kidneys in macaques infected with *P. putida*.

Studies have shown that urinary tract infections are a common problem in *Pseudomonas* sp. infections. Bacteraemia may occur with lower urinary tract manipulation, whereas ascending urinary tract infections may result in pyelonephritis and renal damage. Congestion can occur when the infection causes swelling and irritation of the blood vessels in the kidney. Dilated blood vessels disrupt blood flow to organs and tissues, causing congestion that may lead to the formation of lumps called granulomas, which can damage the surrounding area. This process can affect the kidneys and lead to chronic kidney disease and kidney failure (Mittal *et al*. 2009). Haemorrhages were observed in the podocytes of Bowman's capsule and the distal convoluted tubules.

Infiltration of inflammatory cells in the kidney is known as glomerulonephritis, which occurs when the internal structure of the kidney (the glomeruli) becomes inflamed. This condition can be acute or chronic and causes the loss of protein from the blood and white and red blood cells to leak from the blood into the urine (Montgomerie *et al*. 1980).

Based on the results, the conclusions are that the lesion in the lung organs indicated by pneumonia alveolar, followed by several necrosis, congestion, and haemorrhages, are indicated by Pseudomonas putida infection. The lungs were the organs most affected by possible infection, whereas the kidneys were the least affected. A molecular study for *Pseudomonas putida* diagnosis should be performed to improve the diagnosis and characterisation of this infection. A better marker of the lesion by immunohistochemistry (IHC) will provide details about the type of lesion corresponding to the infection.

References

Al-Mossawai, O.F., Ali, A.H. 2019. Histopathological changes in the liver and spleen of common Carp *Cyprinus carpio* L. challenge with *Pseudomonas aeruginosa* (Schroeter, 1872) fed with dietary chitosan and ciprofloxacin. *Basrah J. Agric. Sci.*, 32(2), 193-207.

Allen, M.S. 2003. Multiple benign lung tumours. *Semin Thorac Cardiovasc Surg*., 15(3), 310-314.

Ashdown, L.R., Guard, R.W. 1984. The prevalence of human melioidosis in Northern Queensland. *Am. J. Trop. Med. Hyg*., 33(3), 474-8.

Baraaj, A.H., Al-Mathkury, H.J. 2013. Histopathological changes in spleen caused by *Pseudomonas aeruginosa* DNA. *J. Biol. Sci*., 3(8), 319-324.

Blazevic, D.J., Koepcke, M.H., Matsen, J.M. 1973. Incidence and identification of *Pseudomonas fluorescens* and *Pseudomonas putida* in the clinical laboratory. *Appl. Microbiol*., 25, 107-110.

Brancatelli, G., Furlan, A., Calandra, A., Dioguardi, B.M. 2018. Hepatic sinusoidal dilatation. *Abdom. Radiol.* , 43(8), 2011-2022.

Bruguera, M., Aranguibel, F., Ros, E., Rodés, J. 1978. Incidence and clinical significance of sinusoidal dilatation in liver biopsies. *Gastroenterol*, 75(3), 474-478.

Carpenter, R.J., Hartzell, J.D., Forsberg, J.A., Babel, B.S., Ganesan, A. 2008. *Pseudomonas putida* war wound infection in a US Marine: a case report and review of the literature. *J. Infect.*, 56, 234-240.

Ceridon, M., Wanner, A., Johnson, B.D. 2009. Does the bronchial circulation contribute to congestion in heart failure?. *Med. Hypothesis*, 73(3), 414-419.

Dijkstra, C.D,, Veerman, A.J.P., Jones, T.C., Ward, J.M., Mohr, U., Hunt, R.D. 1990. Normal anatomy, histology, ultrastructure, rat monographs on pathology of laboratory animals: Hematopoietic system. In Jones, T.C., Mohr, U., Hunt, R.D. (Ed.), *Monographs on pathology of laboratory animals* (pp. 192-204). Berlin, DE: Springer.

Erol, S., Zencirovglu, A., Dilli, D., Okumuks, N., Aydin, M., Göl, N. 2014. Evaluation of nosocomial blood stream infections caused by *Pseudomonas* species in newborns. *Clin. Lab*., 60, 615-620.

Farver, C.F. 2018. Bacterial disease. In Zander, D.S., Farver, C.F. (2nd ed.), *Pulmonary pathology* (pp. 163-200). Amsterdam, NL: Elsevier.

Fernández, M., Niqui-Arroyo, J.L., Conde, S., Ramos, J.L., Duque, E. 2012. Enhanced tolerance to naphthalene and enhanced rhizoremediation performance for *Pseudomonas putida* KT2440 via the NAH7 catabolic plasmid. *Appl. Environ. Microbiol*., 78, 5104-5110.

Fetzer, A.E., Werner, A.S., Hagstrom, J.W.C. 1967. Pathologic features of pseudomonal pneumonia. *Am. Rev. Respir. Dis*., 96, 1121-1130

Hussain, A.N., Kumar, V., Abbas, A.K., Fausto, N. 2005. Robbins and Cotran: Pathologic basis of disease (7th ed). China: Elsevier.

Kim, S.E., Park, S.H., Park, H.B., Park, K.H., Kim, S.H., Jung, S.I., Shin, J.H., Jang, H.C., Kang, S.J. 2012. Nosocomial *Pseudomonas putida* bacteraemia: high rates of carbapenem resistance and mortality. *Chonnam Med. J*., 48(2), 91-95.

Krasnogorskiĭ, I.N., Indikova, M.G., Tsinzerling, V.F., Boĭkov, S.G. 1983. Pathologic anatomy of *Pseudomonas aeruginosa* infections in children. *Arkhiv Patologii*, 45(10), 9-14.

Lefkowitch, J.H. 2007. Liver biopsy assessment in chronic hepatitis. *Arch. Med. Res*., 38(6), 634-643.

Löffler, B., Niemann, S., Ehrhardt, C. 2014. Pathogenesis of *Staphylococcus aureus* necrotizing pneumonia. *Expert Rev. Anti Infect Ther*., 11(10), 1041-1051.

Lombardi, G., Luzzaro, F., Docquier, J.D., Riccio, M.L., Perilli, M.C.A. 2002. Nosocomial infections caused by multidrug-resistant isolates of *Pseudomonas putida* producing VIM-1 metallo-beta-lactamase. *J. Clin. Microbiol*., 40, 4051-4055.

Ludwig, J., Batts, K.P. 1998. Practical liver biopsy interpretation: Diagnostic algorithms (2nd ed.). California: Amer Society of Clinical.

Martino, R., Martínez, C., Pericas, R., Salazar, R., Solá, C., Brunet, S. 1996. Bacteraemia due to glucose non-fermenting gram-negative bacilli in patients with haematological neoplasia and solid tumours. *Eur. J. Clin. Microbiol. Infect. Dis*., 15, 610-615.

Mays, B.B., Thomas, G.D., Leonard, J.S., Pierce, A.K. 1969. Gram negative bacillary necrotising pneumonia: A bacteriologic and histopathologic correlation. *J. Infect Dis*., 120, 687-697.

Mittal, R., Aggarwal, S., Sharma, S., Chhibber, S., Harjai, K. 2009. Urinary tract infections caused by *Pseudomonas aeruginosa*: a minireview. *J. Infect Pub. Health*, 2(3), 101-111.

Molina, L., Udaondo, Z., Duque, E., Fernández, M., Molina-Santiago, C., Roca, A. 2014. Antibiotic resistance determinants in a *Pseudomonas putida* strain isolated from a hospital. *PloS One*, 9(1), 81604.

Montgomerie, J.Z., Tuddenham, W.J., Howard, E.B., Morrow, J.W. 1980. *Pseudomonas* urinary tract infection in mice. *Infect Immun*., 29(1), 267-270.

Oh, W.T., Kim, J.H., Jun, J.W., Giri, S.S., Yun, S., Kim, H.J., Kim, S.G., Kim, S.W., Han, S.J., Kwon, J., Park, S.C. 2019. Genetic characterisation and pathological analysis of a novel bacterial pathogen, *Pseudomonas tructae*, in rainbow trout (*Oncorhynchus mykiss*). *Microorganisms*, 7(10), 432.

Palleroni, N.J. 1984. Genus I. *Pseudomonas*. In Kriland, N.R, Holt, J.G., *Bergey's manual of systemic bacteriology* (pp.141-199). Baltimore: Williams and Wilkins.

Shaheed, H.S., Faleh, E.B. 2018. Effect of pyocin from *Pseudomonas aeruginosa* on liver and spleen pathology induced by *Leishmania donovani* in BALB/C mice. *Onl. J. Vet. Res*., 22(9), 754-760.

Stefanski, S.A., Elwell, M.R., Stromberg, P.C. 1990. Spleen, lymph nodes, and thymus. In Boorman, G.A., Eustis, S.L., Elwell, M.R., Montgomery, C.A., MacKenzie, W.F. (Eds.), *Pathology of the fischer rat: Reference and atlas* (pp. 369-394). San Diego: Academic Press.

Suttie, A.W. 2006. Histopathology of the spleen. *Toxicol Pathol.*, 34(5), 466-503.

Tillotson, J.R, Lerner, A.M. 1968. Characteristics of nonbacteremic *Pseudomonas* pneumonia. *Ann. Intern. Med*., 68, 295-307

Udaondo, Z., Molina, L., Daniels, C., Gómez, M.J., Molina, Henares, M.A, Matilla, M.A, Roca, A., Fernández, M., Duque, E., Segura, A., Ramos, J.L. 2013. Metabolic potential of the organic-solvent tolerant *Pseudomonas putida* DOT-T1E deduced from its annotated genome. *Microb. Biotechnol*., 6(5), 598-611.

Yoshino, Y., Kitazawa, T., Kamimura, M., Tatsuno, K., Ota, Y., Yotsuyanagi, H. 2011. *Pseudomonas putida* bacteraemia in adult patients: Five case reports and a review of the literature. *J. Infect. Chemotherm*., 17, 278-282.